Developmental Cell
Article

Cdc42 Mediates Bmp-Induced Sprouting Angiogenesis through Fmnl3-Driven Assembly of Endothelial Filopodia in Zebrafish

Yuki Wakayama,[1] Shigetomo Fukuhara,[1,*] Koji Ando,[1] Michiyuki Matsuda,[2,3] and Naoki Mochizuki[1,4]
[1]Department of Cell Biology, National Cerebral and Cardiovascular Center Research Institute, Fujishirodai 5-7-1, Suita, Osaka 565-8565, Japan
[2]Laboratory of Bioimaging and Cell Signaling, Graduate School of Biostudies, Kyoto University, Sakyo-ku, Kyoto 606-8501, Japan
[3]Department of Pathology and Biology of Diseases, Graduate School of Medicine, Kyoto University, Sakyo-ku, Kyoto 606-8501, Japan
[4]JST-CREST, National Cerebral and Cardiovascular Center, Fujishirodai 5-7-1, Suita, Osaka 565-8565, Japan
*Correspondence: fuku@ncvc.go.jp
http://dx.doi.org/10.1016/j.devcel.2014.11.024

SUMMARY

During angiogenesis in vivo, endothelial cells (ECs) at the tips of vascular sprouts actively extend filopodia that are filled with bundles of linear actin filaments. To date, signaling pathways involved in the formation of endothelial filopodia have been studied using in-vitro-cultured ECs that behave differently from those in vivo. Herein, we have delineated a signaling pathway that governs the assembly of endothelial filopodia during angiogenic sprouting of the caudal vein plexus (CVP) in zebrafish. During CVP formation, bone morphogenetic protein induces the extension of endothelial filopodia and their migration via Arhgef9b-mediated activation of Cdc42. Active Cdc42 binds to and stimulates Formin-like 3, an actin-regulatory protein of the formin family, which, in turn, promotes the extension of endothelial filopodia to facilitate angiogenic sprouting of the CVP. Thus, this study has elucidated molecular mechanisms underlying the formation of endothelial filopodia and their role in angiogenesis in vivo.

INTRODUCTION

Angiogenesis refers to the physiological and pathological processes through which new blood vessels form from pre-existing ones. During in vivo angiogenesis, endothelial tip cells at the fronts of the growing vessels actively extend filopodia in the direction of cell migration in response to guidance cues (Gerhardt et al., 2003; De Smet et al., 2009). Filopodia are thin, finger-like protrusions that are filled with tight parallel bundles of filamentous actin (F-actin) and function as antennae allowing cells to probe their microenvironment (Mellor, 2010; Mattila and Lappalainen, 2008). Consequently, filopodia play an important role in numerous cellular processes, including cell migration, wound healing, cell adhesion to the extracellular matrix, chemotactic axon guidance, and embryonic development (De Smet et al., 2009; Mattila and Lappalainen, 2008; Mellor, 2010). Therefore, it is believed that filopodia on endothelial tip cells lead the way for vessel growth by sensing guidance cues during angiogenesis. However, this notion was challenged by a recent study showing that inhibition of the formation of filopodia did not affect guided migration of endothelial cells (ECs) but did decrease their migration velocity during angiogenesis (Phng et al., 2013). These results imply that filopodia are required for efficient EC migration during angiogenesis but are not necessary for endothelial tip cell guidance. Therefore, the mechanisms by which EC filopodia regulate angiogenesis in vivo remain unknown.

The Rho family small GTPases regulate actin cytoskeleton reorganization, thereby controlling cell morphology and motility (Heasman and Ridley, 2008). Among these proteins, Cdc42 promotes the formation of filopodia, whereas RhoA and Rac1 induce the formation of stress fibers and lamellipodia, respectively. Two models, convergent elongation and tip nucleation, have been proposed to underlie the formation of filopodia (Mellor, 2010; Mattila and Lappalainen, 2008). The tip nucleation model involves filopodial actin filaments being directly nucleated at filopodial tips by formins. Formin-family proteins promote the assembly of linear actin filaments and are required to generate cellular actin structures such as filopodia and stress fibers (Higgs, 2005; Watanabe and Higashida, 2004; Yang and Svitkina, 2011). Among these proteins, mDia2 (also known as DIAPH3) and Formin-like protein 3 (FMNL3, also known as FRL2) have been shown to induce the formation of filopodia (Yang and Svitkina, 2011; Peng et al., 2003; Harris et al., 2010). mDia2 is autoinhibited via an intramolecular interaction between its N- and C-terminal regions, which masks the formin homology (FH) 1 and FH2 catalytic domains. Active Cdc42 binds to the N-terminal GTPase binding domain (GBD) of mDia2, which prevents the autoinhibitory interaction, thereby promoting the assembly of linear actin filaments (Mellor, 2010; Mattila and Lappalainen, 2008). However, the activation mechanism of FMNL3 remains unknown.

Rho GTPases are involved in the regulation of EC morphology and motility (Lamalice et al., 2007; De Smet et al., 2009). Vascular endothelial growth factor (VEGF) regulates EC migration and actin cytoskeleton via activation of Rac1 and Cdc42 (Soga et al., 2001; Garrett et al., 2007; Lamalice et al., 2007). However, our current knowledge regarding the mechanism of EC migration is based only on the results of in vitro studies, in which ECs never

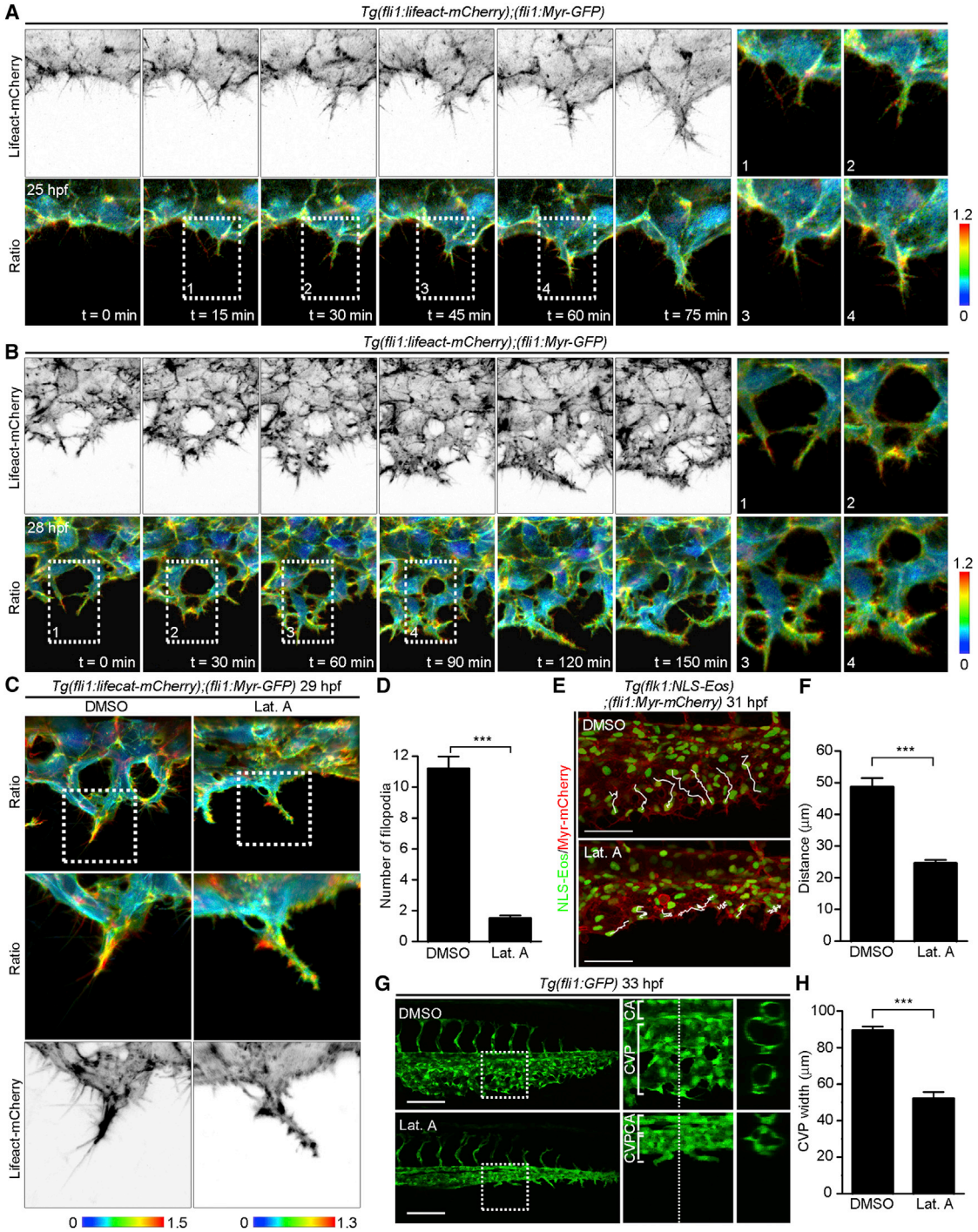

Figure 1. Filopodia Are Required for EC Migration during CVP Formation

(A and B) 3D-rendered confocal images of the CVP of *Tg(fli1:lifeact-mCherry);(fli1:Myr-GFP)* embryos at 25 hpf (A) and 28 hpf (B) and their subsequent time-lapse images at the indicated time points. Upper row: mCherry images (intensity of Lifeact-mCherry is shown as a grayscale image); lower row, mCherry/GFP ratio images shown in the IMD mode (Ratio). The upper and lower limits of the ratio range are indicated on the right. The boxed areas labeled with numbers 1–4 are enlarged on the right side.

(C) 3D-rendered confocal images of the CVP of *Tg(fli1:lifeact-mCherry);(fli1:Myr-GFP)* embryos treated with DMSO or 0.1 μg/ml Lat. A from 26 to 29 hpf. Top: ratio images of mCherry/GFP; middle: enlarged images of the boxed areas; bottom: enlarged mCherry images of the boxed areas. The upper and lower limits of the ratio range are indicated on the bottom.

(D) The number of filopodia for each EC located at the vascular front, as observed in (C), was quantified as described in the Experimental Procedures and shown as the mean ± SEM (DMSO, n = 10; Lat. A, n = 12).

(legend continued on next page)

extend long filopodia as observed in vivo. Thus, the mechanisms by which Rho GTPases regulate the extension of EC filopodia during in vivo angiogenesis remain unknown.

Here, we used in vivo fluorescence-based bioimaging techniques using zebrafish and delineated the signaling pathway that governs the formation of EC filopodia in angiogenic sprouting of the caudal vein plexus (CVP). Cdc42 is activated by bone morphogenetic protein (Bmp) through Arhgef9b (also known as Collybistin) and promotes Fmnl3-mediated formation of EC filopodia, thereby facilitating sprouting angiogenesis during CVP formation.

RESULTS

Filopodial Formation Is Required for EC Migration during Caudal Vein Formation

To investigate the molecular mechanisms underlying EC morphology and motility during angiogenesis, we focused on the morphogenic processes involving caudal veins (CVs), since their formation occurs through sprouting angiogenesis. For CV development, ECs must sprout from CV primordia, migrate ventrally at approximately 27 hr postfertilization (hpf), and form the CVP through the process of angiogenesis at 36 hpf (Figure S1A available online). To analyze actin cytoskeleton dynamics in ECs during angiogenesis, we have developed a double transgenic (Tg) zebrafish line that expresses C-terminally mCherry-tagged lifeact, a small actin-binding peptide (Riedl et al., 2008) and myristoylation signal (Myr)-tagged GFP under the control of the EC-specific *fli1* promoter *Tg(fli1:lifeact-mCherry);(fli1:Myr-GFP)* by exploiting the Tol2 transposon system (Figures S1B and S1C). ECs on the ventral side of the CV primordia showed repeated extension and retraction of small and short-lived filopodia and started to migrate ventrally by producing a single, long, thick filopodium (Figure 1A; Figure S1D; Movie S1). During this ventral migration, the ECs led by filopodia anastomosing with each other formed the CVP (Figure 1B; Movie S2). Filopodia extending from migrating ECs were filled with linear actin filaments (Figures 1A and 1B). F-actin was also detected at cell-cell junctions and in the cell cortex (Figures 1A and 1B).

We next investigated whether linear F-actin assembly and the extension of filopodia in ECs are required for CVP formation. It was previously reported that low concentrations of actin polymerization inhibitor block the formation of EC filopodia in zebrafish (Phng et al., 2013). Consistently, the embryos treated with 0.1 μg/ml latruncullin A (Lat. A), a toxin that prevents actin polymerization by binding to actin monomers (Morton et al., 2000), exhibited disruption of linear F-actin and subsequent breakdown of filopodia in the ECs forming the CV (Figures 1C and 1D). Moreover, ventral migration of ECs and CVP formation were inhibited by Lat. A treatment (Figures 1E–1H; Movie S3). These results indicate linear F-actin assembly and the subsequent formation of filopodia to be responsible for ventral migration of ECs during CVP formation.

Bmp Promotes EC Extension to Form Filopodia, Thereby Regulating CVP Formation

Bmp2b promotes venous angiogenesis to form the CV through activation of Bmp receptor type II (Bmpr2) a/b and activin receptor-like kinase 2/3 (Alk2/3) heterotetrameric receptor complexes (Wiley et al., 2011). Thus, we investigated the role of Bmp in the formation of filopodia by EC during CVP development by examining the effect of a Bmp antagonist, Noggin3. For this purpose, *Tg(fli1:lifeact-mCherry);(fli1:Myr-GFP)* embryos were injected with *heat shock protein* (*hsp*)*70l:noggin3-FLAG* plasmid at the one-cell stage and then heat shocked at 22 hpf for 2 hr. Overexpression of Noggin3 reduced the number of sprouts from the CV primordia and that of filopodia extending from the ECs in the CV primordia, thereby leading to defective CVP formation (Figures 2A–2C; Figure S2A). To clarify the role of Bmp signaling in ECs, we analyzed *Tg(fli1:Gal4FF);(fli1:Myr-mCherry)* embryos injected with a *UAS:GFP,bmpr1ΔC-FLAG* Tol2 plasmid, which drives the expression of GFP and a dominant-negative mutant of Bmpr1 (Bmpr1ΔC-FLAG) simultaneously in ECs (Figure S2B). Bmpr1ΔC-FLAG-expressing ECs failed to localize on the ventral side of the CVP, indicating that endothelial Bmp signaling is required for ventral migration of ECs during CVP formation (Figures 2D and 2E). In contrast, Hsp-mediated overexpression of Bmp2b induced dorsal sprouting of ECs from the CVP, leading to the formation of ectopic venous vessels (Figure S2C; Movie S4). In the ectopic sprouts, ECs actively produced numerous filopodia that were filled with linear F-actin, although their cell morphology differed from that of the ventrally migrating ECs (Figure 2F). Lat. A disrupted filopodia in sprouting ECs and prevented the formation of ectopic venous vessels (Figures 2G–2J). These results suggest that Bmp is involved in the extension of filopodia by EC during CVP formation.

Recently, Dunworth et al. (2014) showed that Bmp signaling suppresses lymphatic cell fate specification through miR-31- and miR-181a-mediated downregulation of Prox1a, a key regulator of lymphatic EC differentiation, raising the possibility that Bmp might induce EC to form filopodia by negatively regulating lymphatic EC development. To address this possibility, we examined the effect of Noggin3 on CVP formation in embryos depleted of Prox1a. Overexpression of Noggin3 resulted in the inhibition of CVP formation in both control morpholino

(E) Projection view of confocal z stack images of the CVP of *Tg(flk1:NLS-Eos);(fli1:Myr-mCherry)* embryos treated with DMSO or Lat. A from 25 to 31 hpf. The merged images of Eos (green) and mCherry (red) are superimposed on the migration paths of ECs (white lines) inferred from time-lapse confocal movies taken from 25 to 31 hpf.

(F) The EC migration distance, as observed in (E), was quantified and is shown as the mean ± SEM (DMSO, n = 6; Lat. A, n = 6).

(G) Projection view of confocal z stack images of the caudal regions of *Tg(fli1:GFP)* embryos treated with DMSO or Lat. A from 24 to 33 hpf. The boxed areas in the left panel are enlarged in the middle panel. The cross-sectional single-plane images of the areas indicated by dotted lines on the enlarged images are shown in the right column. CA, caudal artery.

(H) The CVP width, as observed in (G), was quantified and is shown as the mean ± SEM (DMSO, n = 8; Lat. A, n = 8).

Scale bars, 50 μm in (E) and (G). All zebrafish images are shown dorsal to the top and anterior to the left, unless otherwise described. ***$p < 0.001$. See also Figure S1 and Movies S1, S2, and S3.

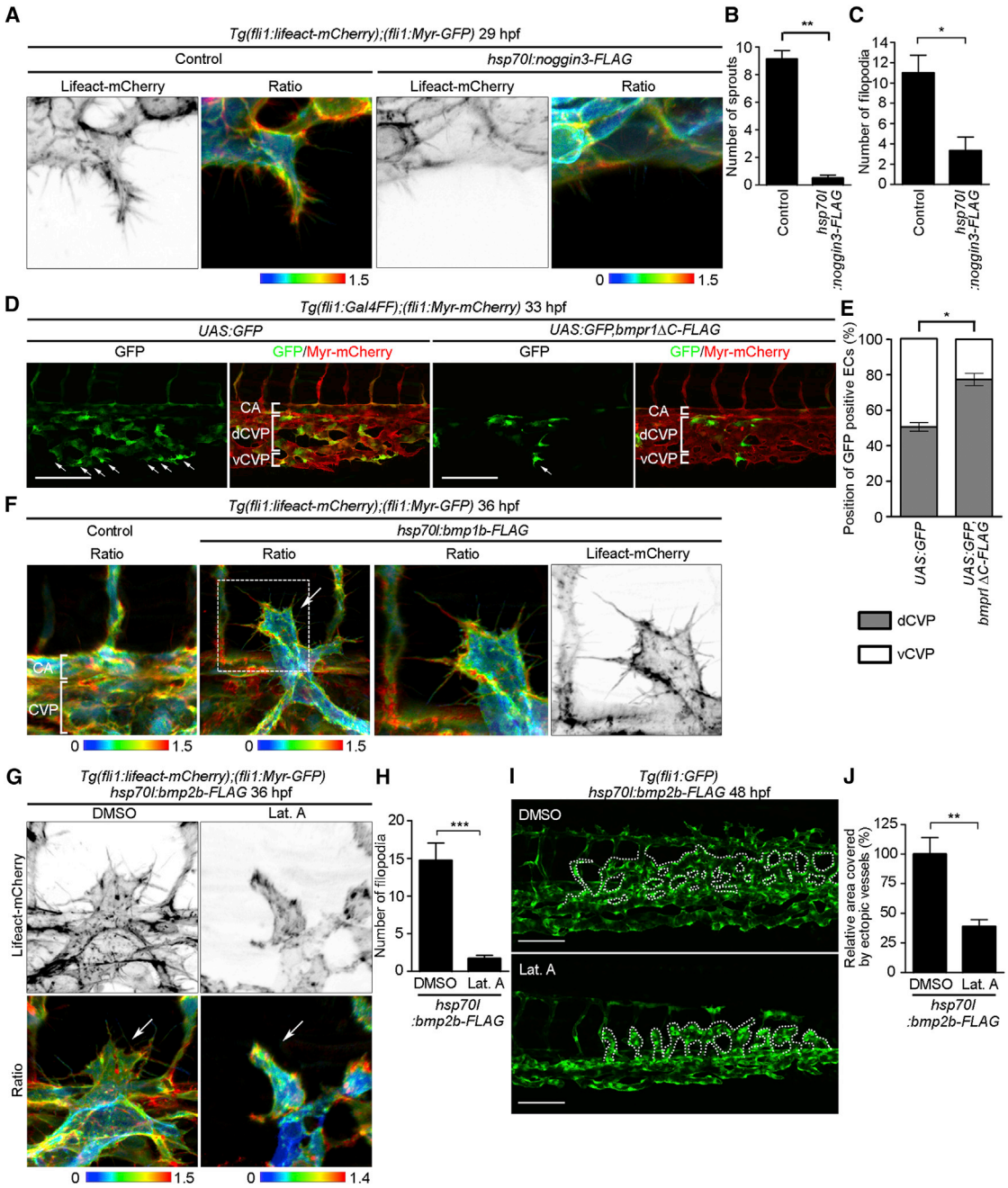

Figure 2. Bmp Induces EC to Extend into Filopodia during CVP Formation

(A) 3D-rendered confocal 3D images of the CVP of 29 hpf *Tg(fli1:lifeact-mCherry);(fli1:Myr-GFP)* embryos injected without (Control) or with *hsp70l:noggin3-FLAG*-Tol2 plasmid and heat shocked at 22 hpf for 24 hr are shown as in Figure 1A.

(B) The total number of sprouts extending from the CV primordia, as observed in (A), was counted and is shown as the mean ± SEM (Control, n = 5; *hsp70l:noggin3-FLAG*, n = 4).

(C) The number of filopodia for each EC located at the vascular front, as observed in (A), was quantified as in Figure 1D (Control, n = 5; *hsp70l:noggin3-FLAG*, n = 4). Error bars indicate means ± SEM.

(D) Projection view of confocal z stack images of the caudal regions of 33 hpf *Tg(fli1:Gal4FF);(fli1:Myr-mCherry)* embryos injected with *UAS:GFP* Tol2 vector (*UAS:GFP*) or *UAS:GFP,bmpr1ΔC-FLAG* Tol2 plasmid (*UAS:GFP,bmpr1ΔC-FLAG*). Left, GFP images; right, the merged images of GFP (green) and mCherry (red). Arrows indicate GFP-expressing ECs that localize in the ventral part of CVP. CA, caudal artery; dCVP, dorsal part of CVP; vCVP, ventral part of CVP.

(E) Percentages of GFP-expressing ECs localizing in the dCVP or vCVP, as observed in (D), are shown as means ± SEM (*UAS:GFP*, n = 6; *UAS:GFP, bmpr1ΔC-FLAG*, n = 5).

(F) 3D-rendered confocal images of the caudal regions of 36 hpf *Tg(fli1:lifeact-mCherry);(fli1:Myr-GFP)* embryos injected without (Control, left panel) or with *hsp70l:bmp2b-FLAG* Tol2 plasmid (right three panels) and heat shocked at 24 hpf for 30 min are shown as in Figure 1A. The mCherry/GFP ratio and mCherry images of the boxed area are enlarged in the third and fourth panels from the left, respectively. Arrow indicates ectopic venous vessels.

(legend continued on next page)

oligonucleotide (MO)-injected and *prox1a* MO-injected embryos, although *prox1a* morphants exhibited defects in thoracic duct formation (Figures S2D–S2F). Moreover, knockdown of miR-31 and miR-181a did not affect the formation of ectopic venous vessels induced by overexpression of Bmp2a (Figures S2G and S2H). These findings indicate that Bmp induces EC extension of filopodia during CVP formation independently of its role in EC fate determination.

Cdc42 Induces EC Extension of Filopodia during CVP Formation

Among the Rho family GTPases, Cdc42 is involved in the formation of filopodia. To investigate whether Cdc42 regulates the formation of filopodia by EC during sprouting angiogenesis in vivo, we visualized the localization of active Cdc42 in ECs by analyzing *Tg(fli1:Gal4FF)* embryos injected with a *UAS:mCherry,GFP-N-WASP CRIB* Tol2 plasmid, which drives the expression of mCherry and the GFP-tagged Cdc42/Rac interactive binding domain (CRIB) of neural Wiskott-Aldrich syndrome protein (GFP-N-WASP CRIB) simultaneously in ECs. GFP-N-WASP CRIB, but not its mutant incapable of binding Cdc42 (GFP-N-WASP CRIB H211D), was clearly accumulated in the filopodia, which extended from sprouting ECs during CVP formation (Figures 3A–3D). Consistently, Cdc42 activation in EC filopodia was also confirmed by the analyses using a fluorescence resonance energy transfer (FRET)-based biosensor for Cdc42 (Figures S3A–S3E) (Komatsu et al., 2011; Ando et al., 2013). These results indicate that Cdc42 is activated in the filopodia produced by the sprouting ECs during CVP formation.

To investigate the role of Cdc42 in EC extension to form filopodia, we analyzed embryos injected with 5 ng *cdc42* MO, in which Cdc42 expression was partially downregulated (Figure S3F). These morphants appeared morphologically normal but clearly exhibited defects in CVP formation, which was partially normalized by injecting MO-resistant *cdc42* mRNA (Figures 3E and 3F; Figure S3G). Consistently, a partial depletion of Cdc42 reduced the number of sprouts from CV primordia, as well as that of filopodia extending from ECs during CVP formation (Figures 3G–3I), indicating that Cdc42 regulates EC extension to form filopodia during CVP development. However, *cdc42* morphants also exhibited decreased numbers of ECs in the CVP (Figures S3H and S3I). Therefore, Cdc42 might regulate not only EC morphology and motility but also EC proliferation and/or survival during CVP formation.

To confirm the role of Cdc42 in EC extension to form filopodia during CVP development, we specifically inhibited the endothelial Cdc42-dependent signal by expressing the membrane-targeted form of ACK42 (Myr-GFP-ACK42) in ECs. ACK42 is a Cdc42-specific inhibitor derived from ACK1 that specifically binds to the active form of Cdc42 (Figure S3J) (Nur-E-Kamal et al., 1999). In Tg zebrafish embryos in which Myr-GFP-ACK42 was specifically expressed in ECs, the ECs in the CV primordia failed to extend to form filopodia (Figures S3K and S3L). We further examined embryos that exhibited mosaic expression of GFP, Myr-GFP-ACK42, or GFP-tagged dominant-negative mutant of Cdc42 (GFP-Cdc42 T17N) in ECs (Figures 3J–3L; Figures S3M and S3N; Movie S5). During CVP formation, more than 70% of ECs expressing either Myr-GFP-ACK42 or GFP-Cdc42 T17N failed to migrate ventrally and remained on the dorsal side of the CVP. Collectively, these results indicate that Cdc42 promotes EC extension to form filopodia and their migration to regulate CVP formation. Consistently, an in vitro EC spheroid-sprouting assay also revealed that Cdc42 is required for EC sprouting (Figures S3O and S3P).

Bmp Regulates CVP Formation through Arhgef9b, a Guanine Nucleotide Exchange Factor for Cdc42

Ets1-related protein (Etsrp), a transcription factor involved in vascular development, induces the expressions of guanine nucleotide exchange factors (GEFs) for Cdc42, including Arhgef9b and Fgd5 (Gomez et al., 2009). We investigated whether these GEFs function in Cdc42-mediated extension of filopodia during CVP formation. In situ hybridization analyses revealed *arhgef9b* and *fgd5* mRNAs to be exclusively expressed in the vasculature of zebrafish embryos (Figure 4A; Figure S4A). Most notably, *arhgef9b* mRNA was highly expressed in the CV primordia and CVP of 24 and 30 hpf embryos, respectively (Figure 4A). Knockdown of Arhgef9b by MO resulted in an impairment of CVP formation, whereas *fgd5* morphants showed normal CVP structures (Figures 4B and 4C; Figures S4B–S4G). Depletion of Arhgef9b also reduced the number of sprouts from CV primordia and that of filopodia extending from ECs during CVP formation (Figures 4D–4F). These results suggest Arhgef9b as a Cdc42 GEF to play a role in CVP formation. Consistently, overexpression of GFP-tagged Arhgef9b (GFP-Arhgef9b) in 293T cells activated Cdc42 but not RhoA or Rac1 (Figure S4H). Furthermore, the impaired CVP formation observed in the *arhgef9b* morphants was normalized by injecting MO-resistant mRNA encoding GFP-Arhgef9b but not by injecting MO-resistant mRNA encoding the corresponding catalytically inactive mutant GFP-Arhgef9b 4A (Figures 4B and 4C; Figure S4I). These results suggest that Arhgef9b, but not Fgd5, activates Cdc42 to regulate CVP formation.

We next investigated whether Arhgef9b acts downstream from Bmp to regulate CVP formation. Depletion of Arhgef9b significantly suppressed Bmp2b-induced formation of ectopic vessels (Figures 4G and 4H). We further determined the genetic interaction between Bmp signaling and Arhgef9b during CVP

(G) 3D-rendered confocal images of the caudal regions of 36 hpf *Tg(fli1:lifeact-mCherry);(fli1:Myr-GFP)* embryos injected with *hsp70l:bmp2b-FLAG* Tol2 plasmid, heat shocked at 24 hpf for 30 min and treated with DMSO or Lat. A from 29 to 33 hpf are shown as in Figure 1A. Arrows indicate ectopic venous vessels.
(H) The number of filopodia for each EC located at the front of ectopic vessels, as observed in (G), was quantified as in Figure 1D (DMSO, n = 7; Lat. A, n = 7). Error bars indicate means ± SEM.
(I) Projection view of confocal z stack images of the caudal regions of 48 hpf *Tg(fli1:GFP)* embryos injected with *hsp70l:bmp2b-FLAG* Tol2 plasmid, heat shocked at 24 hpf for 30 min, and treated with DMSO or Lat. A from 33 to 48 hpf. Dotted lines indicate ectopic venous vessels.
(J) The areas covered by ectopic venous vessels as observed in (I) were quantified and expressed as percentages relative to that observed in DMSO-treated embryos. Data are shown as means ± SEM (DMSO, n = 5; Lat. A, n = 5).
Scale bars, 100 μm in (D) and (I). *$p < 0.05$; **$p < 0.01$; ***$p < 0.001$. See also Figure S2 and Movie S4.

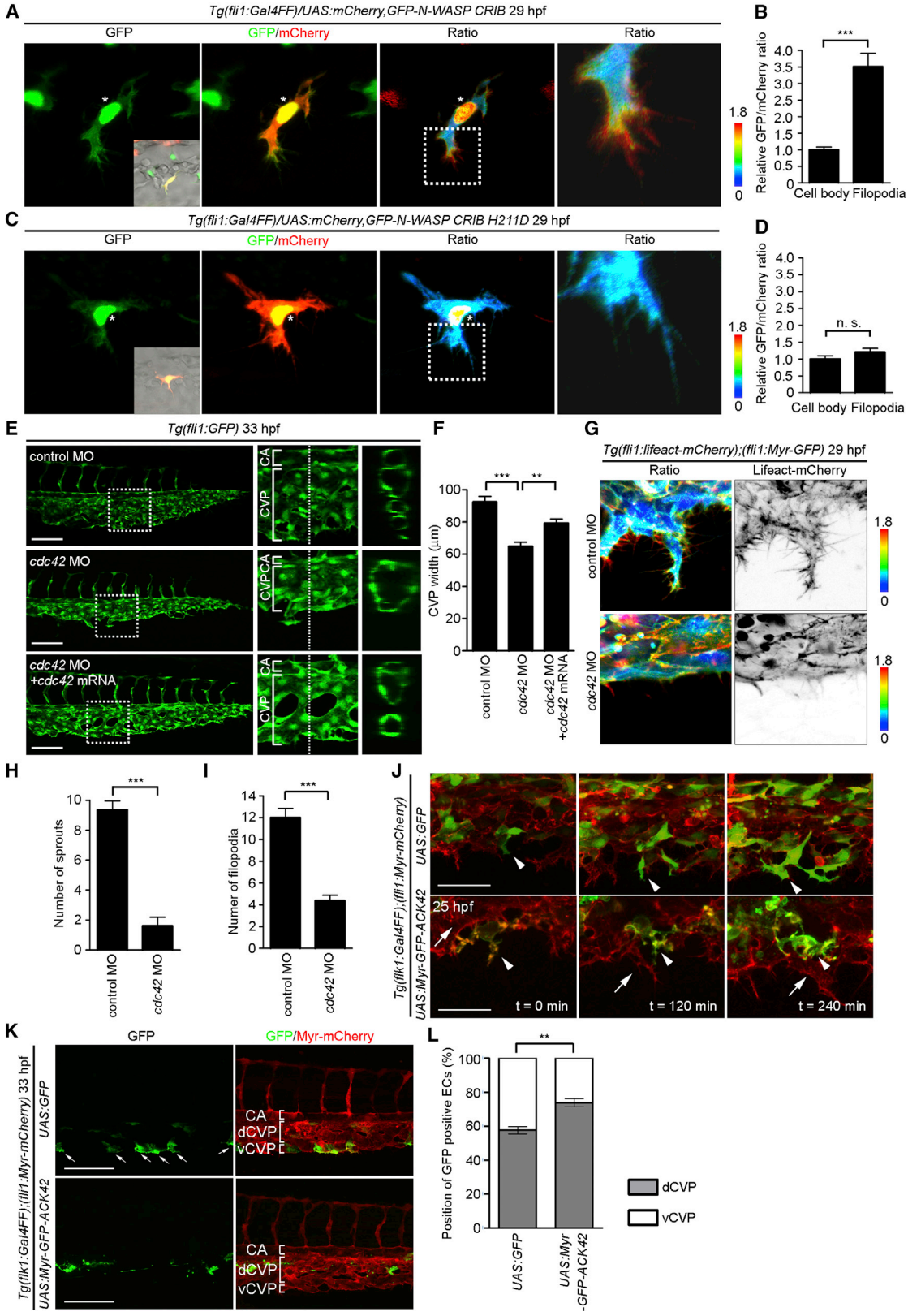

Figure 3. Cdc42 Mediates EC Extension into Filopodia during CVP Formation

(A) 3D-rendered confocal images of the ECs in the CVP of 29 hpf *Tg(fli1:Gal4FF)* embryos injected with *UAS:mCherry,GFP-N-WASP CRIB* Tol2 plasmid. The GFP image, the merged image of GFP (green) and mCherry (red) (GFP/mCherry), and the GFP/mCherry ratio image, in the IMD mode (Ratio), are shown as indicated at

(legend continued on next page)

formation by using MOs targeting two Bmpr2 receptors (*bmpr2a* and *bmpr2b)* and *arhgef9b*. Injection of a low dose of either a combination of *bmpr2a* MO (1 ng) and *bmpr2b* MOs (0.5 ng) or *arhgef9b* MO alone (0.5 ng) into zebrafish embryos did not affect CVP formation, while a high dose of either MO (a combination of 5 ng of *bmpr2a* and 2.5 ng of *bmpr2b* MOs or 2.5 ng of *ahrgef9b* MO) clearly inhibited CVP formation (Figures 4I and 4J). However, coinjection of a low dose of *bmpr2a* or *bmpr2b* MOs with the *arhgef9b* MO impaired CVP formation (Figures 4I and 4J). These findings suggest that Bmp is likely to be involved in the regulation of Cdc42-mediated extension of filopodia and CVP formation by Arhgef9b.

Fmnl3-Driven Actin Polymerization Is Required for EC Extension to Form Filopodia during CVP Development

We investigated the molecular mechanism underlying Cdc42-mediated filopodia extension during CVP formation. Filopodia formation is believed to be driven by assembly of linear F-actin. Among regulators of the actin cytoskeleton, formin family proteins are known to regulate the formation of linear unbranched actin (Higgs, 2005; Watanabe and Higashida, 2004; Yang and Svitkina, 2011). Therefore, we first investigated whether formin family proteins are involved in EC extension to form filopodia during CVP development. Treatment with a formin inhibitor, SMIFH2 (Rizvi et al., 2009), disrupted EC filopodia and prevented CVP formation (Figures 5A–5D), suggesting the involvement of formin family proteins in these processes.

In mammals, 15 members of the formin family of proteins have been identified. To investigate which of these proteins are involved in the formation of filopodia by ECs, we analyzed their expressions by RT-PCR in three human EC lines (Figure S5A). Expressions of *FMNL2*, *FMNL3*, *FHOD1*, *DIA1*, *DIAPH3*, and *INF2* were detected in all EC lines. Among these proteins, FMNL3 has been shown to regulate angiogenesis, although its role in actin cytoskeleton regulation in ECs has not been studied (Hetheridge et al., 2012). Thus, we explored whether Fmnl3 and its homologous isoforms, Fmnl2a and Fmnl2b, are involved in CVP formation. In situ hybridization analyses revealed *fmnl3* mRNA to be exclusively expressed in vascular ECs, while *fmnl2a* and *fmnl2b* mRNAs were broadly expressed in zebrafish embryos (Figure S5B). RT-PCR analyses of GFP-positive ECs isolated from *Tg(fli1:GFP)* embryos suggested predominantly *fmnl3*, but, weakly, other formin-like proteins such as *fmnl1*, *fmnl2a*, and *fmnl2b*, to be expressed by the ECs in zebrafish embryos (Figure S5C). Furthermore, CVP formation was significantly inhibited by knocking down Fmnl3 but not by knockdown of Fmnl2a or Fmnl2b (Figures 5E and 5F; Figures S5D–S5I). Defective CVP formation observed in *fmnl3* morphants was normalized by injecting MO-resistant *fmnl3* mRNA (Figures 5E and 5F), indicating the essential role of Fmnl3 in CVP formation. Moreover, we investigated the cause of the CVP defects observed in *fmnl3* morphants. The number of ECs in the CVP of *fmnl3* morphants was not different from that in the CVP of control MO-injected embryos, indicating that Fmnl3 is not required for EC proliferation and survival during CVP formation (Figures S5J and S5K). However, the ECs failed to produce filopodia and sprout from the CV primordia in *fmnl3* morphants (Figures 5G–5I; Movie S6). Furthermore, ECs expressing a dominant-negative mutant of Fmnl3 (Fmnl3 I684A-GFP), in which the FH2 catalytic domain is mutated, could not localize on the ventral side of the CVP, indicating the requirement of Fmnl3 for ventral migration of ECs during CVP formation (Figures 5J and 5K). Consistently, an in vitro EC spheroid-sprouting assay also revealed the requirement of Fmnl3 for EC sprouting (Figures S5L and S5M). In a Tg zebrafish line that expresses Fmnl3-GFP in ECs, Fmnl3-GFP was

the top. The boxed area in the Ratio image is enlarged on the far right side. The inset in the GFP image is the single-scan merged image of differential interference contrast GFP and mCherry images. The upper and lower limits of the ratio range are indicated on the right. Note that accumulation of GFP-N-WASP CRIB in the nucleus indicated by asterisks does not reflect localization of GTP-Cdc42, since its mutant, which is incapable of binding GTP-bound Cdc42 (GFP-N-WASP CRIB H211D), was also accumulated in the nucleus as shown in (C).

(B) Relative GFP/mCherry ratio (localization of GTP-Cdc42) in the filopodia and cell bodies of ECs located at the vascular front in the CVP, as observed in (A), was expressed as the fold increase relative to that observed in the cell body. Data are shown as means ± SEM (n = 15).

(C) 3D-rendered confocal images of the EC in the CVP of 29 hpf *Tg(fli1:Gal4FF)* embryos injected with *UAS:mCherry,GFP-N-WASP CRIB H211D* Tol2 plasmid are shown as in (A).

(D) Relative GFP/mCherry ratio in the filopodia and cell bodies of ECs located at the vascular front in the CVP, as observed in (C), is shown as in (B) (n = 13). Error bars indicate means ± SEM.

(E) Projection view of confocal z stack images of the caudal regions of 33 hpf *Tg(fli1:GFP)* embryos injected with 5 ng control MO (upper panel), 5 ng *cdc42* MO (middle panel), and 5 ng *cdc42* MO together with 100 pg MO-resistant *cdc42* mRNA (lower panel) are shown as in Figure 1G.

(F) The CVP width, as observed in (E), was quantified and is shown as the mean ± SEM (control MO, n = 6; *cdc42* MO, n = 5; *cdc42* MO + *cdc42* mRNA, n = 5).

(G) 3D-rendered confocal images of the CVP of 29 hpf *Tg(fli1:lifeact-mCherry);(fli1:Myr-GFP)* embryos injected with 5 ng control MO (upper panels) and 5 ng *cdc42* MO (lower panels) are shown as in Figure 1A.

(H) The number of sprouts extending from the CV primordia, as observed in (G), was quantified as in Figure 2B (control MO, n = 6; *cdc42* MO, n = 5). Error bars indicate means ± SEM.

(I) The number of filopodia for each EC located at the vascular front, as observed in (G), was quantified as in Figure 1D (control MO, n = 10; *cdc42* MO, n = 11). Error bars indicate means ± SEM.

(J) Projection view of confocal z stack images of the CVP of *Tg(flk1:Gal4FF-2A-mCherry);(fli1:Myr-mCherry)* embryos injected with *UAS:GFP*-Tol2 plasmid or *UAS:Myr-GFP-ACK42*-Tol2 plasmid at 28 hpf and subsequent time-lapse images at the indicated time points. The merged images of GFP (green) and mCherry (red) are shown. Arrowheads and arrows indicate GFP-positive and GFP-negative ECs, respectively. Note that Myr-GFP-ACK42-expressing ECs failed to migrate during CVP formation.

(K) Projection views of confocal z stack images of the caudal regions of 33 hpf *Tg(flk1:Gal4FF-2A-mCherry);(fli1:Myr-mCherry)* embryos injected with *UAS:GFP* Tol2 plasmid or *UAS:Myr-GFP-ACK42* Tol2 plasmid are shown as in Figure 2D.

(L) Percentages of GFP-expressing or Myr-GFP-ACK42-expressing ECs localized in the dorsal part of the CVP (dCVP) or the ventral part of the CVP (vCVP), as observed in (K), are shown as means ± SEM (GFP, n = 8; Myr-GFP-ACK42, n = 9).

Scale bars, 100 μm in (E) and (K) and 50 μm in (J). **p < 0.01; ***p < 0.001; n.s., no significance. See also Figure S3 and Movie S5.

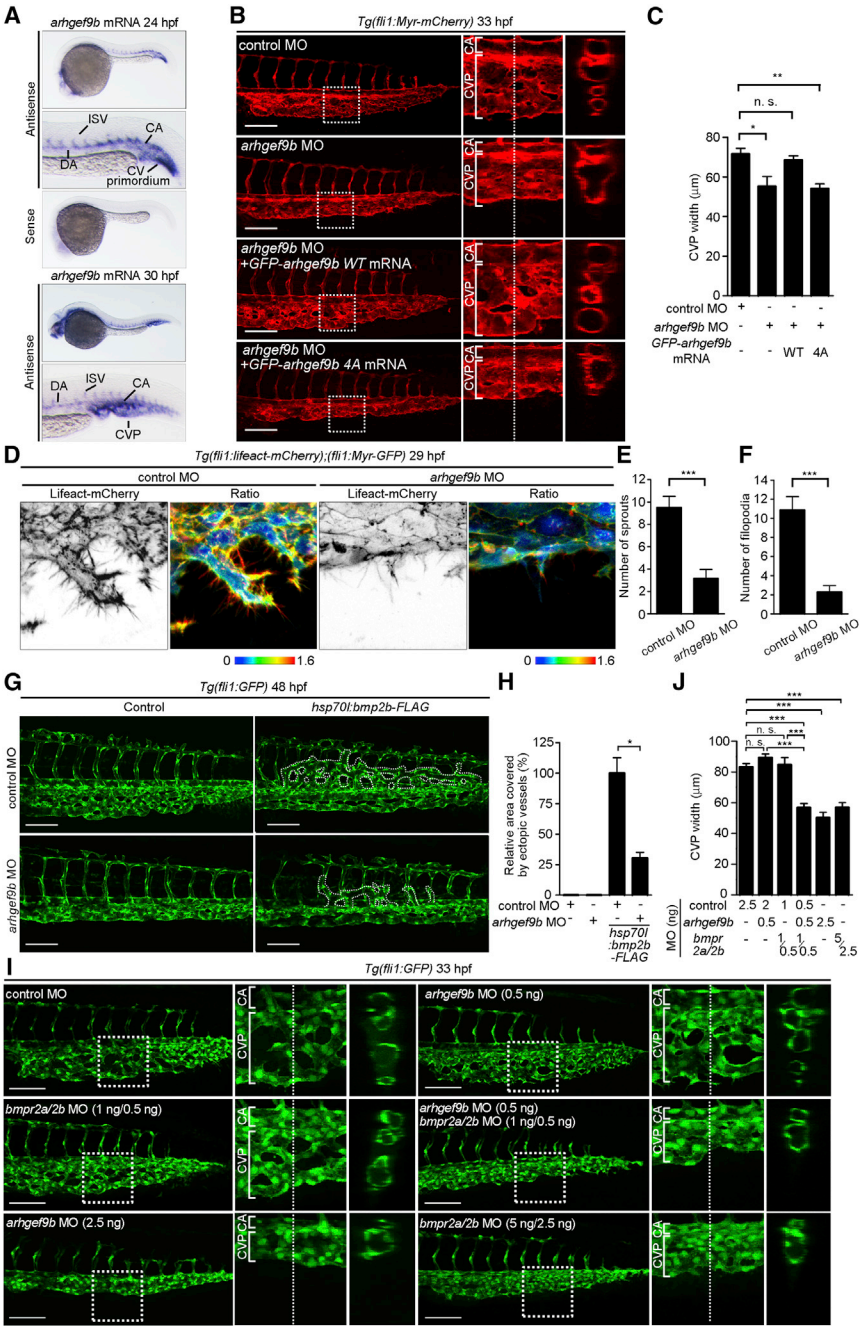

Figure 4. Arhgef9b, a Cdc42 GEF, Is Involved in Bmp-Mediated CVP Formation

(A) Expression patterns of *arhgef9b* mRNA in zebrafish embryos at 24 and 30 hpf as detected by whole-mount in situ hybridization. The caudal region is enlarged in the lower panel. A sense probe was used to confirm the specificity of the hybridization reaction. DA, dorsal aorta; CA, caudal artery.

(B) Projection views are shown of confocal z stack images of the caudal regions of 33 hpf *Tg(fli1:Myr-mCherry)* embryos injected with 2.5 ng control MO, 2.5 ng *arhgef9b* MO, and 2.5 ng *arhgef9b* MO, together with either 100 pg MO-resistant *GFP-arhgef9b* mRNA or 100 pg MO-resistant *GFP-arhgef9b 4A* mRNA as in Figure 1G.

(C) The CVP width, as observed in (B), was quantified as in Figure 1H (control MO, n = 13; *arhgef9b* MO, n = 11; *arhgef9b* MO + *GFP-arhgef9b WT* mRNA [WT], n = 14; and *arhgef9b* MO + *GFP-arhgef9b 4A* mRNA [4A], n = 5). Error bars indicate means ± SEM.

(D) 3D-rendered confocal images of the CVP of 29 hpf *Tg(fli1:lifeact-mCherry);(fli1:Myr-GFP)* embryos injected with 5 ng control MO and 5 ng *arhgef9b* MO are shown as in Figure 1A.

(E) The number of sprouts extending from the CV primordia, as observed in (D), was quantified as in Figure 2B (control MO, n = 8; *arhgef9b* MO, n = 7). Error bars indicate means ± SEM.

(F) The number of filopodia for each EC located at the vascular front, as observed in (D), was quantified as in Figure 1D (control MO, n = 8; *arhgef9b* MO, n = 7). Error bars indicate means ± SEM.

(G) Projection view of confocal z stack images of the caudal regions of 48 hpf *Tg(fli1:GFP)* embryos injected with 2.5 ng control MO (upper panel) or 2.5 ng *arhgef9b* MO (lower panel), either alone (Control) or together with *hsp70l:bmp2b-FLAG* Tol2 plasmid. Dotted lines indicate ectopic venous vessels.

(H) The areas covered by ectopic venous vessels, as observed in (G), were quantified and expressed as percentages relative to that observed in the embryos injected with both control MO and *hsp70l:bmp2b-FLAG* Tol2 plasmid. Data are shown as means ± SEM (each sample, n = 12).

(I) Projection view of confocal z stack images of the caudal regions of 33 hpf *Tg(fli1:GFP)* embryos injected with control MO, both *bmpr2a* and *bmp2rb* MOs, and *arhgef9b* MO, as indicated in the upper left corner of each image, are shown as in Figure 1G. The amounts of injected MOs (per embryo) are also indicated in parentheses after the name of the MO.

(J) The CVP width, as observed in (I), was quantified as in Figure 1H (n ≥ 5). Error bars indicate means ± SEM.

Scale bars, 100 μm in (B), (G), and (I). *p < 0.05; **p < 0.01; ***p < 0.001; n.s., no significance. See also Figure S4.

localized in filopodia extending from ECs during CVP formation (Figure 5L). Taken together, these results indicate that Fmnl3 regulates CVP formation by inducing EC extension, to form filopodia, and migration.

Fmnl3 Acts Downstream from the Bmp-Arhgef9b Signaling Axis to Regulate CVP Formation

Next, we investigated whether the Bmp-Arhgef9b signaling axis utilizes Fmnl3 to regulate CVP formation. Bmp2b-induced formation of ectopic venous vessels was suppressed by depletion of Fmnl3 (Figures S6A and S6B). The embryos injected with either a low dose of *bmpr2a* (1 ng)/*bmpr2b* (0.5 ng) MOs or a low dose of *fmnl3* MO (1 ng) exhibited normal CVP formation (Figures S6C and S6D). However, coinjection of both MOs significantly inhibited CVP formation, indicating a genetic interaction between Bmp signaling and Fmnl3. Similarly, CVP formation was not affected by the injection of either a low dose of *arhgef9b* MO (1 ng) or a low dose of *fmnl3* MO (1 ng) into zebrafish

embryos but was significantly impeded by coinjection of both MOs (Figures S6E and S6F). These findings suggest that Fmnl3 acts downstream from the Bmp-Arhgef9b signaling pathway to regulate CVP formation.

Cdc42 Promotes Fmnl3-Mediated Extension of EC Filopodia during CVP Formation

Finally, we investigated how Cdc42 induces Fmnl3-mediated extension of filopodia. Diaphanous-related formins (Drfs), a subfamily of the formin proteins, are thought to be autoinhibited by intramolecular interaction between their own N- and C-terminal regions. Binding of active Rho GTPases to the N-terminal GBD prevents this autoinhibitory intramolecular interaction to promote actin assembly (Watanabe and Higashida, 2004; Pollard, 2007; Higgs, 2005). Since Fmnl3 is a member of the Drf family (Figure 6A), we hypothesized that Fmnl3 might be similarly autoinhibited in a manner dependent on an intramolecular interaction between different regions of the same Drfs. The GFP-tagged C-terminal region of Fmnl3 (Fmnl3 C-ter-GFP), but not the GFP-tagged FH1-FH2 domain of Fmnl3 (Fmnl3 FH1/FH2-GFP), was coimmunoprecipitated with the FLAG-tagged N-terminal region of Fmnl3 (Fmnl3 N-ter-FLAG) (Figure 6B). Furthermore, either Fmnl3 C-ter-GFP or Fmnl3 FH1/FH2-GFP significantly induced actin polymerization when overexpressed in human umbilical vein ECs (HUVECs), although GFP-tagged wild-type (WT) Fmnl3 (Fmnl3 WT-GFP) had no effect on actin organization (Figures 6C and 6D). However, coexpression of Fmnl3 N-ter-FLAG apparently blunted the actin polymerization induced by Fmnl3 C-ter-GFP but not that induced by Fmnl3 FH1/FH2-GFP (Figures 6C and 6D). In addition, actin assembly was promoted by the Fmnl3 mutant lacking the C-terminal diaphanous autoregulatory domain (DAD) (Fmnl3 ΔDAD-GFP) (Figures 6C and 6D). These results indicate that the actin polymerization activity of Fmnl3 is autoinhibited by the intramolecular interaction between the N-terminal region and the C-terminal DAD.

Next, we explored whether autoinhibition of Fmnl3 is prevented by Rho GTPases by examining the association of Fmnl3 N-ter-FLAG containing GBD with Rho GTPases. The active form of Cdc42, but not that of either RhoA or Rac1, bound to the N-terminal region of Fmnl3 (Figure 7A). In addition, low-level expression of the active form of Cdc42, although it did not itself affect organization of the actin cytoskeleton, synergistically induced actin polymerization with WT Fmnl3 (Figures 7B and 7C). In contrast, neither RhoA nor Rac1 functioned with Fmnl3-GFP to induce actin polymerization (Figures 7B and 7C). Moreover, Fmnl3-GFP was broadly localized to the plasma membrane when expressed in ECs, while coexpression of active Cdc42 relocated Fmnl3-GFP in the filopodia (Figure S7A). These results suggest Fmnl3 activity to be increased by binding of Cdc42 to its own N-terminal region.

To confirm this observation, we constructed two plasmids encoding the mutants of Fmnl3: the Fmnl3 I111D-GFP mutant, which is incapable of binding to Cdc42 but retains the capacity for the intramolecular interaction (Figures S7B and S7C), and the Fmnl3 I684A-GFP mutant in which the FH2 catalytic domain is mutated. Unlike WT Fmnl3, the Fmnl3 I111D-GFP and Fmnl3 I684A mutants did not induce actin polymerization cooperatively with Cdc42 (Figures S7D–S7G). Moreover, CVP defects caused by Fmnl3 deficiency were normalized by expression of WT Fmnl3 but not by that of either the Fmnl3 I111D mutant or the Fmnl3 I684A mutant (Figures 7D and 7E; Figures S7H–S7K). Collectively, these findings indicate that Cdc42 induces the Fmnl3-deriven assembly of EC filopodia through its binding to the N-terminal region of Fmnl3, thereby promoting CVP formation.

DISCUSSION

During sprouting angiogenesis, ECs located at the front of growing vessels actively extend filopodia in the direction of cell migration in response to guidance cues. Our present results demonstrate a crucial role for Cdc42-mediated formation of EC filopodia in sprouting angiogenesis during CVP formation and further delineate the signaling pathways that act upstream and downstream from Cdc42 by exploiting in vivo fluorescence-based bioimaging techniques. Cdc42 is activated by Bmp through Arhgef9b and promotes EC migration by inducing Fmnl3-mediated formation of EC filopodia, thereby facilitating sprouting angiogenesis during CVP formation.

Bmp-induced extension of EC filopodia may not be involved in EC guidance during angiogenic sprouting of CVP. Filopodia are believed to act as antennae that can sense gradients of guidance cues during directional cell migration. It has also been reported that filopodia extending from endothelial tip cells lead the way by sensing a VEGF gradient during angiogenic sprouting in the early postnatal retina (Gerhardt et al., 2003). In this study, we found that Hsp-mediated ubiquitous expression of Bmp2b did not impair angiogenic sprouting of CVP, although the formation of ectopic venous vessels was induced. Furthermore, Bmp2b, an angiogenic factor responsible for CVP formation, is expressed not only in the tissues surrounding the CVP but also in CV primordia, indicating that there is no Bmp gradient (Wiley et al., 2011). These results suggest that Bmp does not function as a guidance cue but rather may instead increase the motility of ECs during CVP formation. Thus, other factors, such as the extracellular matrix or repulsive guidance cues, might regulate directional EC migration during CVP formation.

Actin polymerization may regulate Bmp-induced EC migration in different ways. Lat. A not only disrupted filopodia but also inhibited EC migration during CVP formation, suggesting that extension of filopodia is required for EC migration during CVP formation. However, inhibition of actin polymerization by Lat. A not only blocks the extension of filopodia but also affects the actomyosin-mediated force generation that is also required for cell movement as well. Therefore, Lat. A might also affect EC migration independently of the disruption of EC filopodia. Thus, detailed examinations are required to elucidate the role of actin polymerization in EC migration during CVP formation.

The extension of filopodia is involved in Bmp-induced EC migration during CVP formation, but it is not required for VEGF-mediated EC migration during intersegmental vessel (ISV) formation. Both filopodia and lamellipodia provide sites for adhesive contacts at the leading edge of migrating cells, thereby promoting cell migration (De Smet et al., 2009; Mattila and Lappalainen, 2008; Mellor, 2010). During VEGF-mediated ISV formation, endothelial tip cells migrated by protruding lamellipodia even when the formation of filopodia was selectively

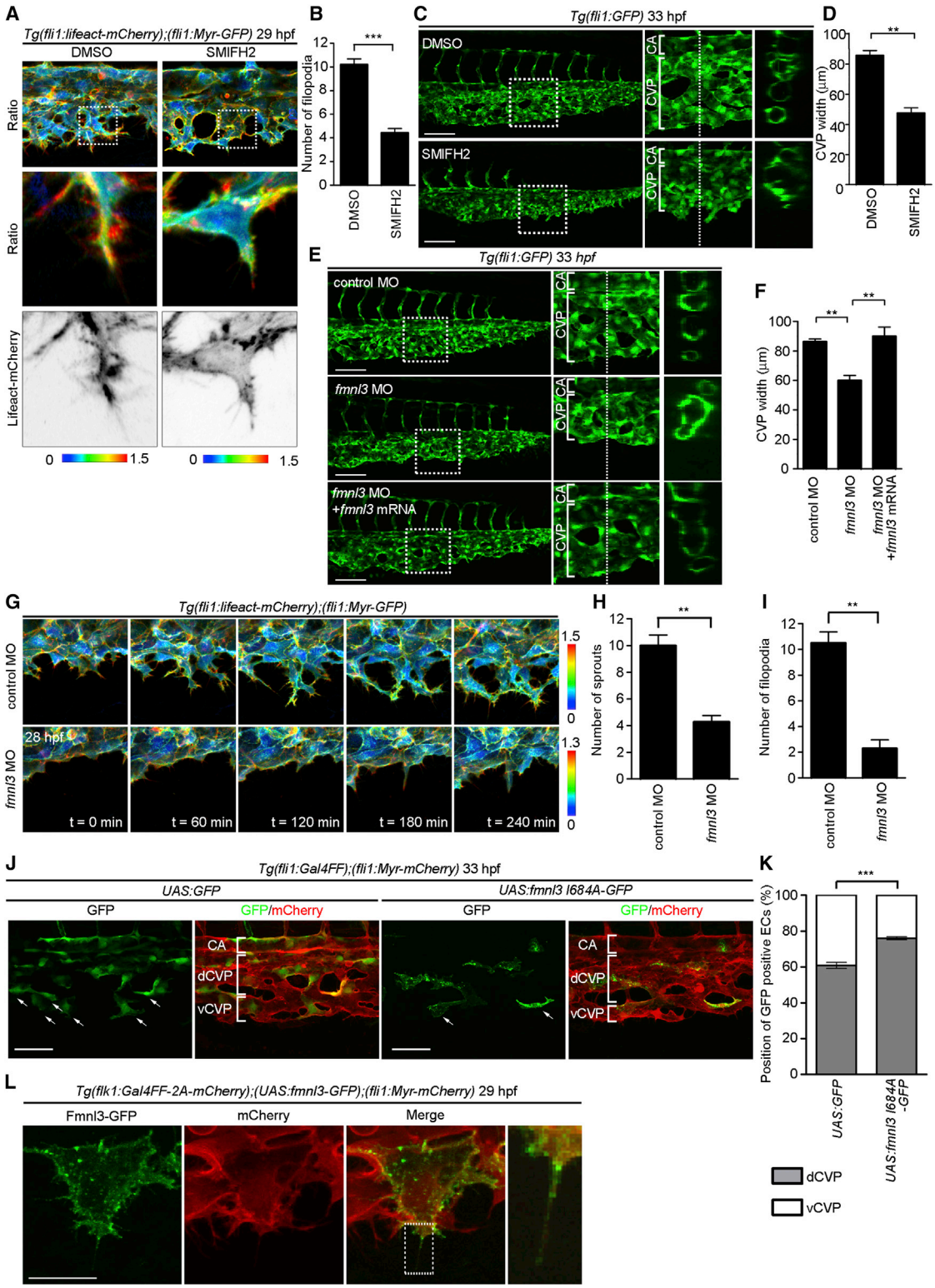

Figure 5. Fmnl3 Is Required for EC to Extend into Filopodia during CVP Formation

(A) 3D-rendered confocal images of the CVP of 29 hpf *Tg(fli1:lifeact-mCherry);(fli1:Myr-GFP)* embryos treated with DMSO or 1 μM SMIFH2, a formin inhibitor, from 25 to 29 hpf are shown as in Figure 1A.

(B) The number of filopodia for each EC located at the vascular front, as observed in (A), was quantified as in Figure 1D (DMSO, n = 10; SMIFH2, n = 12).

(C) Projection view of confocal z stack images of the caudal regions of 33 hpf *Tg(fli1:GFP)* embryos treated with DMSO or SMIFH2 from 24 to 33 hpf are shown as in Figure 1G.

(legend continued on next page)

blocked (Phng et al., 2013). In clear contrast, ECs failed to induce lamellipodial protrusion in the absence of filopodia, thereby leading to defective migration of ECs during Bmp-dependent CVP formation. Thus, filopodia and lamellipodia differentially regulate EC migration during angiogenic sprouting of CVP and ISV; filopodia are essential for Bmp-induced EC migration during CVP formation, whereas VEGF promotes EC migration through the formation of either filopodia or lamellipodia to regulate ISV development. This difference might be attributable to the distinct signaling pathways induced by Bmp and VEGF. Rac1 promotes lamellipodial protrusion, while filopodial extension is induced by Cdc42. Therefore, Bmp might be unable to induce lamellipodial protrusion and EC migration in the absence of filopodia because of its inability to activate Rac1. In contrast, since VEGF can activate both Cdc42 and Rac1, the promotion of EC migration during ISV formation by lamellipodial protrusion may have been possible even in the absence of filopodia. However, further studies are needed to confirm this hypothesis.

Our present data showed that Arghef9b is a Cdc42 GEF that mediates Bmp-induced angiogenesis during CVP formation in zebrafish. However, a role of Arhgef9 in vascular development has not been reported in mammals, although it is known to regulate GABAergic neurotransmission (Harvey et al., 2004; Kins et al., 2000). Indeed, Arhgef9-deficient mice displayed deficits in spatial learning and increased anxiety-like behavior, but the formation of vascular structures was normal (Papadopoulos et al., 2007). Thus, Cdc42 GEFs other than Arhgef9 might be involved in Bmp-induced angiogenesis in mammals.

Fmnl3 induces EC filopodial extension, acting downstream from Cdc42, to regulate CVP formation. Consistently, the FH1-FH2 domain of FMNL3, when overexpressed, is known to promote filopodial formation in multiple cell lines (Harris et al., 2010; Thompson et al., 2013). FMNL3 and its homologs, FMNL1 and FMNL2, constitute a subfamily of Drfs. The Drfs are thought to be held in an autoinhibited state through an intramolecular interaction between their own N- and C-terminal regions (Watanabe and Higashida, 2004; Pollard, 2007; Higgs, 2005). Binding of Rho family GTPases to the N-terminal GBD prevents this autoinhibitory interaction, thereby enabling the FH2 catalytic domain to induce actin polymerization. Consistently, our in vitro analyses revealed that Fmnl3 activity is autoinhibited by an intramolecular interaction between its N-terminal region and the C-terminal DAD and that activation of Fmnl3 is achieved by binding of GTP-loaded Cdc42 to its N-terminal region.

Fmnl3 is required for the angiogenic sprouting of CVP, but it is not essential for that of ISVs. It was previously reported that depletion of Fmnl3 leads to impaired formation of ISVs in zebrafish (Hetheridge et al., 2012). However, we did not observe obvious defects in ISVs in *fmnl3* morphants, although ISV formation appeared to be delayed by Fmnl3 knockdown. Thus, Fmnl3 might be involved in ISV formation, but it is not essential for angiogenic sprouting of ISVs. Phng et al. (2013) recently reported that filopodia are not essential for sprouting angiogenesis during ISV formation, although they are required for efficient EC migration. In clear contrast, the present study revealed filopodia to be indispensable for not only EC migration but also sprouting angiogenesis during CVP formation. Since Fmnl3 is involved in the formation of filopodia, whether Fmnl3 is necessary for sprouting angiogenesis may depend on whether or not filopodia are essential for EC migration during angiogenesis. If so, Fmnl3 might not be required for angiogenic sprouting of ISVs, because filopodia are not essential for EC migration during ISV formation.

In conclusion, the present results indicate that Bmp activates Cdc42 through Arhgef9b, which promotes sprouting angiogenesis during CVP formation by inducing Fmnl3-mediated extension of EC filopodia.

EXPERIMENTAL PROCEDURES

Plasmids

The plasmids used in this study were constructed as described in the Supplemental Experimental Procedures.

Zebrafish and Transgenesis

Zebrafish (*Danio rerio*) were maintained as previously described (Kwon et al., 2013). Animal experiments were approved by the animal committee of the National Cerebral and Cardiovascular Center and performed in accordance with the regulations of the National Cerebral and Cardiovascular Center.

Tg(fli1:Lifeact-mCherry), Tg(fli1:Myr-GFP), Tg(flk1:NLS-Eos), Tg(flk1:mCherry-CAAX), Tg(flk1:Gal4FF-2A-mCherry), Tg(UAS:RaichuEV-Cdc42), Tg(UAS:RaichuEV-Cdc42 NC), Tg(UAS:Myr-GFP-ACK42), and *Tg(UAS:fmnl3-GFP)*

(D) The CVP width, as observed in (C), was quantified as in Figure 1H (DMSO, n = 7; SMIFH2, n = 9). Error bars indicate means ± SEM.
(E) Projection view of confocal z stack images of the caudal regions of 33 hpf *Tg(fli1:GFP)* embryos injected with 2.5 ng control MO (upper panel), 2.5 ng *fmnl3* MO (middle panel), and 2.5 ng *fmnl3* MO together with 100 pg MO-resistant *fmnl3* mRNA (lower panel) are shown as in Figure 1G.
(F) The CVP width, as observed in (E), was quantified as in Figure 1H (control MO, n = 8; *fmnl3* MO, n = 6; *fmnl3* MO + *fmnl3* mRNA, n = 8). Error bars indicate means ± SEM.
(G) 3D-rendered confocal images of the CVP of 28 hpf *Tg(fli1:lifeact-mCherry);(fli1:Myr-GFP)* embryos injected with 2.5 ng control MO or 2.5 ng *fmnl3* MO and their subsequent time-lapse images at the indicated time points. The ratio images of mCherry/GFP are shown as in Figure 1A.
(H) The number of sprouts extending from the CV primordia, as observed in (G), was quantified as in Figure 2B (control MO, n = 8; *fmnl3* MO, n = 8). Error bars indicate means ± SEM.
(I) The number of filopodia for each EC located at the vascular front as observed in (G) was quantified as in Figure 1D (control MO, n = 8; *fmnl3* MO, n = 8). Error bars indicate means ± SEM.
(J) Projection views of confocal z stack images of the caudal regions of 33 hpf *Tg(fli1:Gal4FF);(fli1:Myr-mCherry)* embryos injected with *UAS:GFP* Tol2 vector (*UAS:GFP*) or *UAS:fmnl3 I684A-GFP* Tol2 plasmid (*UAS:fmnl3 I684A-GFP*) are shown as in Figure 2D.
(K) Percentages of GFP-expressing ECs localizing in the dorsal part of CVP (dCVP) or the ventral part of CVP (vCVP), as observed in (J), are shown as mean ± SEM (*UAS:GFP*, n = 3; *UAS:fmnl3 I684A-GFP*, n = 3). Error bars indicate means ± SEM.
(L) Projection view of confocal z stack images of one of the ECs located at the vascular front of the CVP in a *Tg(flk1:Gal4FF-2A-mCherry);(UAS:fmnl3-GFP);(fli1:Myr-mCherry)* embryo at 29 hpf. GFP (Fmnl3-GFP) and mCherry images and the merged image (Merge) are shown as indicated at the top. The boxed area on the merged image is enlarged on the right.
Scale bars, 100 μm in (C) and (E), 50 μm in (J), and 20 μm in (L). **p < 0.01; ***p < 0.001. See also Figure S5 and Movie S6.

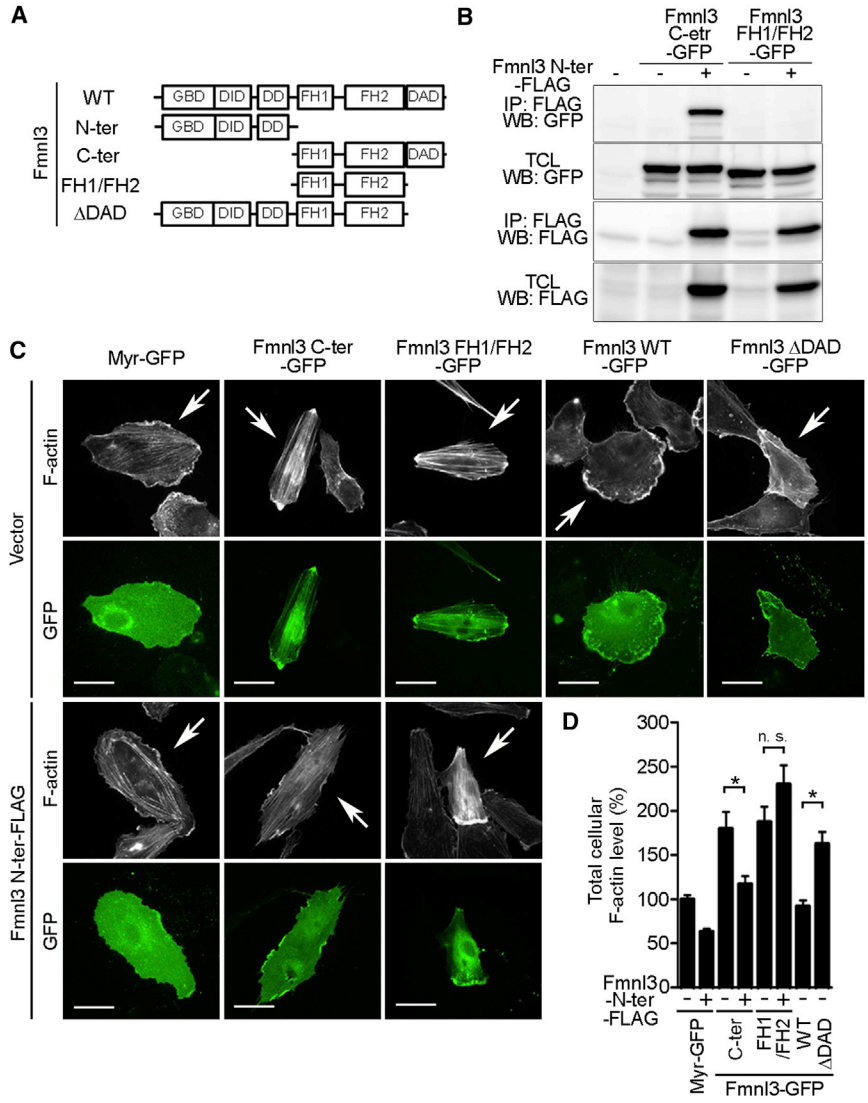

Figure 6. Actin Polymerization Activity of Fmnl3 Is Autoinhibited by Intramolecular Interaction between Its N-Terminal and C-Terminal Regions

(A) Schematic illustrations of Fmnl3 and its mutants. DID, diaphanous inhibitory domain; DD, dimerization domain; ter, terminus.

(B) 293T cells were transfected without (–) or with (+) the plasmid encoding Fmnl3 N-ter-FLAG together with either the plasmid expressing Fmnl3 C-ter-GFP or that encoding Fmnl3 FH1/FH2-GFP as indicated at the top. Immunoprecipitates (IP: FLAG) of cell lysates and total cell lysate (TCL) aliquots were subjected to western blot (WB) analyses with anti-GFP and anti-FLAG antibodies as indicated on the left.

(C) HUVECs transfected with the plasmid encoding Myr-GFP (0.5 μg) or that encoding C-terminally GFP-tagged Fmnl3 (0.5 μg) or its mutants (0.5 μg, Fmnl3 C-ter-GFP, Fmnl3 FH1/FH2-GFP, and Fmnl3 ΔDAD-GFP), as indicated at the top, together with the empty vector (1 μg, Vector) or the plasmid expressing C-terminally FLAG-tagged Fmnl3 N-ter mutant (1 μg, Fmnl3 N-ter-FLAG), as indicated on the left, were stained with rhodamine-phalloidin. The rhodamine (F-actin) and GFP images are shown. Arrows indicate GFP signal-positive cells. Scale bars, 30 μm. Note that expression of either Fmnl3 C-ter-GFP or Fmnl3 FH1/FH2-GFP induced stress fiber formation, while thin actin fibers were formed throughout the cell in response to expression of Fmnl3 ΔDAD-GFP.

(D) Total cellular F-actin levels as observed in (C) were quantified by measuring the rhodamine fluorescence intensity of individual cells and expressed as percentages relative to that observed in Myr-GFP-expressing cells. Data are shown as means ± SEM (n = 17). *p < 0.05; n.s., no significance.

See also Figure S6.

zebrafish lines were generated as described in the Supplemental Experimental Procedures.

Image Acquisition, Processing, and Quantification

The zebrafish embryos were mounted in 1% low-melting agarose poured on a 35-mm-diameter glass-base dish (Asahi Techno Glass), as previously described (Kwon et al., 2013). Confocal images were taken with a FluoView FV1000 confocal upright microscope system (Olympus) with water-immersion 20× (XLUMPlanFL, 1.0 NA) and 40× (LUMPlanFL, 0.80 NA) lenses and equipped with a multi-alkali or a GaAsP photomultiplier tube regulated with FluoView ASW software (Olympus). The 440 nm, 473 nm, and 559 nm laser lines were used. For confocal time-lapse imaging, images were collected every 15 min for 5–10 hr. To avoid cross-detection of green and red signals, images were acquired sequentially at 473 nm and 559 nm. Image files were processed and analyzed using Volocity software (PerkinElmer).

To visualize the localization of F-actin in ECs, mCherry and GFP fluorescence images in the *Tg(fli1:Lifecat-mCherry);(fli1:Myr-GFP)* embryos were acquired. After background subtraction, the mCherry/GFP ratio images were created by Volocity software and displayed as intensity-modulated display (IMD) images.

Similarly, localization of GTP-bound Cdc42 in ECs was visualized by collecting mCherry and GFP images in *Tg(fli1:Gal4FF)* embryos injected with a *UAS:mCherry,GFP-N-WASP CRIB* Tol2 plasmid. After background subtraction, the GFP/mCherry ratio images were created and displayed as IMD images. To quantify the levels of GTP-bound Cdc42 in the filopodia and cell bodies of ECs at the vascular front, a region of interest (ROI) encompassing one filopodium that ventrally extended from the leading edge and a 2-μm-diameter circular ROI drawn in the vicinity of the nucleus of the leading-edge side were used, respectively. The mean emission ratio of GFP/mCherry, calculated by dividing the fluorescence intensity of GFP by that of mCherry in each ROI, was scored as the amount of GTP-Cdc42.

Quantitative image analysis was performed as described in the Supplemental Experimental Procedures.

Heat Shock and Chemical Treatment

To ubiquitously express Noggin3-FLAG and Bmp2b-FLAG, *Tg(fli1:Lifeact-mCherry);(fli1:Myr-GFP)* or *Tg(fli1:GFP)* embryos were injected with 25 ng *pTol2-cmlc2:NLS-mCherry-HS4-hsp70l:noggin3-FLAG* (*hsp70l:noggin3-FLAG*) and 25 ng *pTol2-cmlc2:NLS-mCherry-HS4-hsp70l:bmp2b-FLAG* (*hsp70l:bmp2b-FLAG*) plasmid along with Tol2 transpopase RNA (25 ng), and were heat shocked at 22 hpf for 2 hr and at 24 hpf for 30 min at 39°C, respectively. The embryos carrying the corresponding genes were selected by the expression of mCherry in the nucleus of cardiac myocytes.

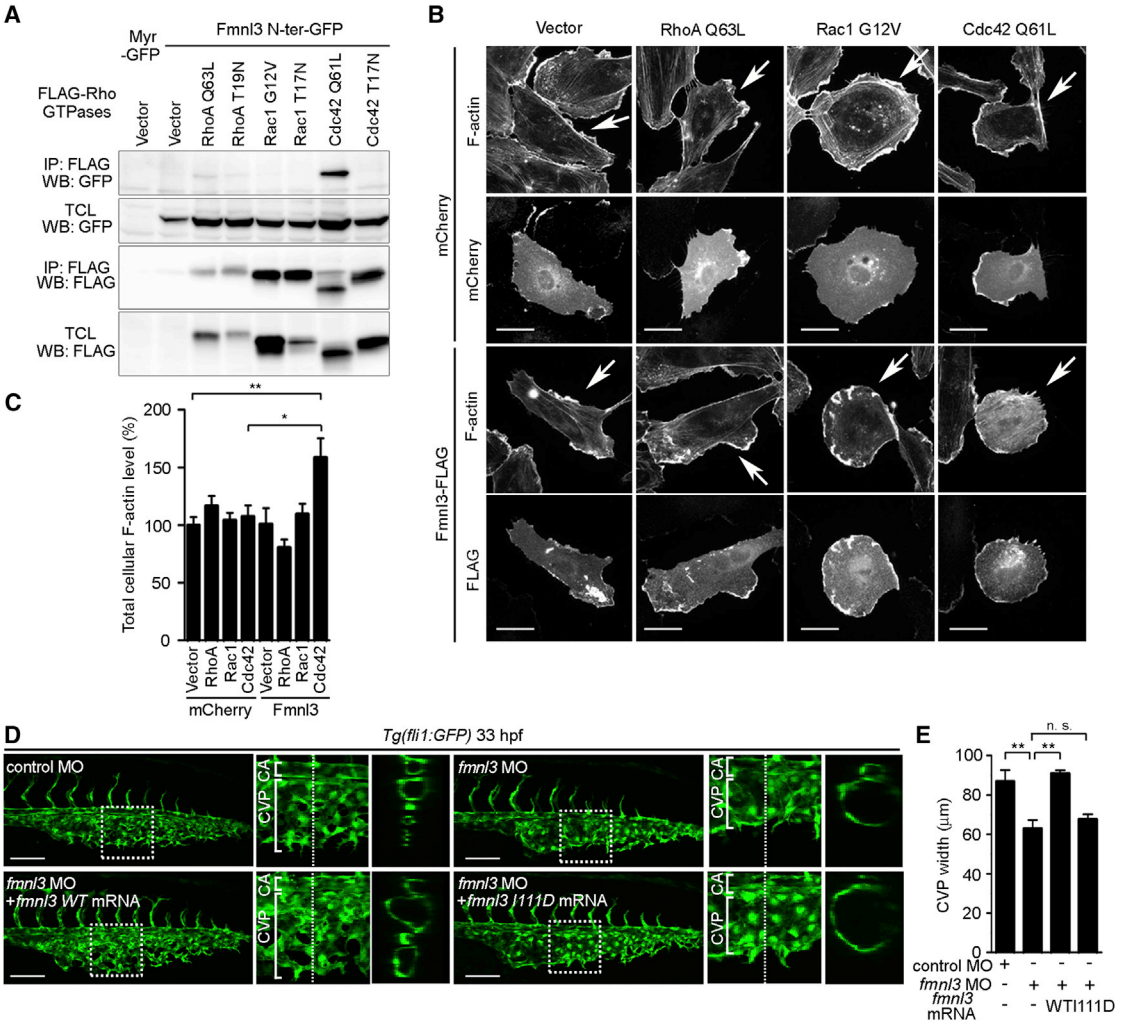

Figure 7. Cdc42 Activates Fmnl3 to Regulate CVP Formation

(A) 293T cells transfected with the plasmid encoding either Myr-GFP or C-terminally GFP-tagged Fmnl3 N-ter mutant (Fmnl3 N-ter-GFP) together with the plasmid encoding FLAG-tagged constitutive active or dominant-negative mutants of Rho GTPases, as indicated at the top, were subjected to coimmunoprecipitation analysis as in Figure 6B. IP, immunoprecipitate; WB, western blot; TCL, total cell lysate.

(B) HUVECs transfected with the plasmid encoding mCherry (1 μg) or that encoding C-terminally FLAG-tagged Fmnl3 (Fmnl3-FLAG, 1 μg) together with empty vector (0.1 μg) or the plasmid expressing RhoA Q63L (0.1 μg), Rac1 G12V (0.1 μg), or Cdc42 Q61L (0.1 μg) were immunostained with anti-FLAG antibody (FLAG) and stained with phalloidin labeled with Alexa Fluor 488 (F-actin). Note that coexpression of Fmnl3-FLAG and Cdc42 Q61L induced the formation of thin actin fibers throughout the cells. Arrows indicate mCherry signal- or FLAG signal-positive cells.

(C) Total cellular F-actin levels, as observed in (B) were quantified as in Figure 6D. Data are expressed as percentages relative to that observed in the cells transfected with empty vector and mCherry-expressing plasmid, and shown as mean ± SEM (n = 16).

(D) Projection view of confocal z stack images of the caudal regions of 33 hpf *Tg(fli1:GFP)* embryos injected with control MO or *fmnl3* MO together with the vehicle or MO-resistant mRNA encoding WT Fmnl3 or Fmnl3 I111D are shown as in Figure 1G.

(E) The CVP width, as observed in (D), was quantified as in Figure 1H ($n \geq 4$). Error bars indicate means ± SEM.

Scale bars, 30 μm in (B) and 100 μm in (D). *$p < 0.05$; **$p < 0.01$; n.s., no significance. See also Figure S7.

Tg(fli1:Lifeact-mCherry);(fli1:Myr-GFP), *Tg(flk1:NLS-Eos);(fli1:Myr-mCherry)*, and *Tg(fli1:GFP)* embryos were dechorinated and incubated in the E3 medium containing 0.1 μM Lat. A and 1 mM SMIFH2 for 23–33 hpf or 25–30 hpf as described in the legends for Figures 1 and 5. As a control, the embryos were also incubated in the E3 medium containing DMSO.

Whole-Mount In Situ Hybridization

Whole-mount in situ hybridization for zebrafish embryos was carried out according to standard procedures as described in the Supplemental Experimental Procedures.

Immunocytochemistry

HUVECs grown in a 35-mm glass-based dish (Asahi Techno Glass) coated with Cellmatrix Type I-C (Nitta Gelatin) were transfected with plasmids, as described in the legends for Figures 6, 7, and S7, and were subjected to immunocytochemistry as described previously (Ando et al., 2013; Fukuhara et al., 2008).

Statistical Analysis

Data were analyzed using GraphPad Prism software (GraphPad Software) and expressed as means ± SEM. Statistical significance for paired samples and for

multiple comparisons was determined using Student's t test and one-way ANOVA with Tukey's test, respectively. Data were considered statistically significant at $p < 0.05$.

SUPPLEMENTAL INFORMATION

Supplemental Information includes Supplemental Experimental Procedures, seven figures, and six movies and can be found with this article online at http://dx.doi.org/10.1016/j.devcel.2014.11.024.

ACKNOWLEDGMENTS

We thank N. Lawson for the plasmid-encoding fli1 promoter and *Tg(fli1:GFP)* fish; K. Kawakami for the Tol2 system and *Tg(UAS:GFP)* fish line; M. Affolter for *Tg(fli1:Gal4FF)* fish; M. Hibi for the Gal4FF plasmid; D.Y. Stainier for the plasmid-encoding flk1 promoter; J. Kuwada for the heat-shock protein 70 promoter; G. Felsenfeld for the chicken β-globin insulator; and D. Kimelman for the Bmpr1 plasmid. We are also grateful to K. Hiratomi, M. Sone, W. Koeda, E. Okamoto, Y. Shintani, and T. Babazono for excellent technical assistance and to K. Shioya for excellent fish care. This work was supported in part by Grants-in-Aid for Scientific Research on Innovative Areas "Fluorescence Live Imaging" (no. 22113009 to S.F.) and "Neuro-Vascular Wiring" (no. 22122003 to N.M.) from the Ministry of Education, Culture, Sports, Science, and Technology in Japan; Grants-in-Aid for Scientific Research (B) (no. 22390040 and no. 25293050 to S.F. and no. 24370084 to N.M.) from the Japan Society for the Promotion of Science; grants from the Ministry of Health, Labour, and Welfare of Japan (to N.M.) and the Core Research for Evolutional Science and Technology Program of the Japan Science and Technology Agency (to N.M.); the Takeda Science Foundation (to S.F. and N.M.); the Naito Foundation (to S.F.); the Mochida Memorial Foundation for Medical and Pharmaceutical Research (to S.F.); and the Japan Cardiovascular Research Foundation (to S.F.).

Received: January 24, 2014
Revised: July 5, 2014
Accepted: November 13, 2014
Published: January 12, 2015

REFERENCES

Ando, K., Fukuhara, S., Moriya, T., Obara, Y., Nakahata, N., and Mochizuki, N. (2013). Rap1 potentiates endothelial cell junctions by spatially controlling myosin II activity and actin organization. J. Cell Biol. *202*, 901–916.

De Smet, F., Segura, I., De Bock, K., Hohensinner, P.J., and Carmeliet, P. (2009). Mechanisms of vessel branching: filopodia on endothelial tip cells lead the way. Arterioscler. Thromb. Vasc. Biol. *29*, 639–649.

Dunworth, W.P., Cardona-Costa, J., Bozkulak, E.C., Kim, J.D., Meadows, S., Fischer, J.C., Wang, Y., Cleaver, O., Qyang, Y., Ober, E.A., and Jin, S.W. (2014). Bone morphogenetic protein 2 signaling negatively modulates lymphatic development in vertebrate embryos. Circ. Res. *114*, 56–66.

Fukuhara, S., Sako, K., Minami, T., Noda, K., Kim, H.Z., Kodama, T., Shibuya, M., Takakura, N., Koh, G.Y., and Mochizuki, N. (2008). Differential function of Tie2 at cell-cell contacts and cell-substratum contacts regulated by angiopoietin-1. Nat. Cell Biol. *10*, 513–526.

Garrett, T.A., Van Buul, J.D., and Burridge, K. (2007). VEGF-induced Rac1 activation in endothelial cells is regulated by the guanine nucleotide exchange factor Vav2. Exp. Cell Res. *313*, 3285–3297.

Gerhardt, H., Golding, M., Fruttiger, M., Ruhrberg, C., Lundkvist, A., Abramsson, A., Jeltsch, M., Mitchell, C., Alitalo, K., Shima, D., and Betsholtz, C. (2003). VEGF guides angiogenic sprouting utilizing endothelial tip cell filopodia. J. Cell Biol. *161*, 1163–1177.

Gomez, G.A., Veldman, M.B., Zhao, Y., Burgess, S., and Lin, S. (2009). Discovery and characterization of novel vascular and hematopoietic genes downstream of etsrp in zebrafish. PLoS ONE *4*, e4994.

Harris, E.S., Gauvin, T.J., Heimsath, E.G., and Higgs, H.N. (2010). Assembly of filopodia by the formin FRL2 (FMNL3). Cytoskeleton (Hoboken) *67*, 755–772.

Harvey, K., Duguid, I.C., Alldred, M.J., Beatty, S.E., Ward, H., Keep, N.H., Lingenfelter, S.E., Pearce, B.R., Lundgren, J., Owen, M.J., et al. (2004). The GDP-GTP exchange factor collybistin: an essential determinant of neuronal gephyrin clustering. J. Neurosci. *24*, 5816–5826.

Heasman, S.J., and Ridley, A.J. (2008). Mammalian Rho GTPases: new insights into their functions from in vivo studies. Nat. Rev. Mol. Cell Biol. *9*, 690–701.

Hetheridge, C., Scott, A.N., Swain, R.K., Copeland, J.W., Higgs, H.N., Bicknell, R., and Mellor, H. (2012). The formin FMNL3 is a cytoskeletal regulator of angiogenesis. J. Cell Sci. *125*, 1420–1428.

Higgs, H.N. (2005). Formin proteins: a domain-based approach. Trends Biochem. Sci. *30*, 342–353.

Kins, S., Betz, H., and Kirsch, J. (2000). Collybistin, a newly identified brain-specific GEF, induces submembrane clustering of gephyrin. Nat. Neurosci. *3*, 22–29.

Komatsu, N., Aoki, K., Yamada, M., Yukinaga, H., Fujita, Y., Kamioka, Y., and Matsuda, M. (2011). Development of an optimized backbone of FRET biosensors for kinases and GTPases. Mol. Biol. Cell *22*, 4647–4656.

Kwon, H.B., Fukuhara, S., Asakawa, K., Ando, K., Kashiwada, T., Kawakami, K., Hibi, M., Kwon, Y.G., Kim, K.W., Alitalo, K., and Mochizuki, N. (2013). The parallel growth of motoneuron axons with the dorsal aorta depends on Vegfc/Vegfr3 signaling in zebrafish. Development *140*, 4081–4090.

Lamalice, L., Le Boeuf, F., and Huot, J. (2007). Endothelial cell migration during angiogenesis. Circ. Res. *100*, 782–794.

Mattila, P.K., and Lappalainen, P. (2008). Filopodia: molecular architecture and cellular functions. Nat. Rev. Mol. Cell Biol. *9*, 446–454.

Mellor, H. (2010). The role of formins in filopodia formation. Biochim. Biophys. Acta *1803*, 191–200.

Morton, W.M., Ayscough, K.R., and McLaughlin, P.J. (2000). Latrunculin alters the actin-monomer subunit interface to prevent polymerization. Nat. Cell Biol. *2*, 376–378.

Nur-E-Kamal, M.S., Kamal, J.M., Qureshi, M.M., and Maruta, H. (1999). The CDC42-specific inhibitor derived from ACK-1 blocks v-Ha-Ras-induced transformation. Oncogene *18*, 7787–7793.

Papadopoulos, T., Korte, M., Eulenburg, V., Kubota, H., Retiounskaia, M., Harvey, R.J., Harvey, K., O'Sullivan, G.A., Laube, B., Hülsmann, S., et al. (2007). Impaired GABAergic transmission and altered hippocampal synaptic plasticity in collybistin-deficient mice. EMBO J. *26*, 3888–3899.

Peng, J., Wallar, B.J., Flanders, A., Swiatek, P.J., and Alberts, A.S. (2003). Disruption of the Diaphanous-related formin Drf1 gene encoding mDia1 reveals a role for Drf3 as an effector for Cdc42. Curr. Biol. *13*, 534–545.

Phng, L.K., Stanchi, F., and Gerhardt, H. (2013). Filopodia are dispensable for endothelial tip cell guidance. Development *140*, 4031–4040.

Pollard, T.D. (2007). Regulation of actin filament assembly by Arp2/3 complex and formins. Annu. Rev. Biophys. Biomol. Struct. *36*, 451–477.

Riedl, J., Crevenna, A.H., Kessenbrock, K., Yu, J.H., Neukirchen, D., Bista, M., Bradke, F., Jenne, D., Holak, T.A., Werb, Z., et al. (2008). Lifeact: a versatile marker to visualize F-actin. Nat. Methods *5*, 605–607.

Rizvi, S.A., Neidt, E.M., Cui, J., Feiger, Z., Skau, C.T., Gardel, M.L., Kozmin, S.A., and Kovar, D.R. (2009). Identification and characterization of a small molecule inhibitor of formin-mediated actin assembly. Chem. Biol. *16*, 1158–1168.

Soga, N., Namba, N., McAllister, S., Cornelius, L., Teitelbaum, S.L., Dowdy, S.F., Kawamura, J., and Hruska, K.A. (2001). Rho family GTPases regulate VEGF-stimulated endothelial cell motility. Exp. Cell Res. *269*, 73–87.

Thompson, M.E., Heimsath, E.G., Gauvin, T.J., Higgs, H.N., and Kull, F.J. (2013). FMNL3 FH2-actin structure gives insight into formin-mediated actin nucleation and elongation. Nat. Struct. Mol. Biol. *20*, 111–118.

Watanabe, N., and Higashida, C. (2004). Formins: processive cappers of growing actin filaments. Exp. Cell Res. *301*, 16–22.

Wiley, D.M., Kim, J.D., Hao, J., Hong, C.C., Bautch, V.L., and Jin, S.W. (2011). Distinct signalling pathways regulate sprouting angiogenesis from the dorsal aorta and the axial vein. Nat. Cell Biol. *13*, 686–692.

Yang, C., and Svitkina, T. (2011). Filopodia initiation: focus on the Arp2/3 complex and formins. Cell Adhes. Migr. *5*, 402–408.